Available online at www.eccomasproceedia.org
Eccomas Proceedia SMART (2023) 390-401

ECCOMAS Proceedia

X ECCOMAS Thematic Conference on Smart Structures and Materials
SMART 2023
D.A. Saravanos, A. Benjeddou, N. Chrysochoidis and T. Theodosiou (Eds)

DESIGN METHODOLOGY OF A COMPOSITE SHEAR RESISTANT FLEXURE FOR A MORPHING STRUCTURE

M.J. MATERMAN[*], S. BENOU[*], L.L. WARNET[*], R.D.R. SITOHANG[*],

W. VAN DER EIJK[†] AND H. VAN GOOZEN[†]

[*] Chair of Production Technology
University of Twente
Drienerlolaan 5, 7522NB, Enschede, the Netherlands
e-mail: l.warnet@utwente.nl, www.utwente.nl

[†] GKN Fokker Aerostructures B.V.
Anthony Fokkerweg 4, 3351 NL Papendrecht, the Netherlands
e-mail: Hans.vanGoozen@fokker.com, www.gknaerospace.com

Abstract.
This paper reports on the methodology behind the development of fiber reinforced thermoplastic flexures meant for a movable morphing application. A concept using a flexible skin and these so-called Shear Resistant Flexure (SRF) connect a fixed wing part to a movable. The SRFs considered should comply to a list of requirements in terms of kinematic, loading, and space. Some of the mechanical constraints combine contradictory elements, like the call for flexibility of an SRF, combined with resistance to shear deformation. Preliminary studies led to a concept based on a thin shell, asking for specific material damage model. This paper proposes a specific type of test, necessary to provide strain allowables in both Quasi-static as in cyclic conditions. These allowables were then used in a Finite Element parametric study to propose a suited geometry for the SRF. Such SRFs were subsequently produced in a small series using state of the art production techniques. The design was then experimentally evaluated.

Key words: Flexure, Compliant Morphing, Thermoplastic Composites

1 INTRODUCTION

The aviation industry is continuously improving the operational performance of aircrafts by increasing their aerodynamic efficiency. A promising way to increase the operational performance of an airplane is by using ‘morphing’ technology. Morphing implies a smooth transition from one shape into another. There are two types of morphing that are studied for the aircraft industry: kinematic morphing and compliant morphing [1, 2]. In kinematic morphing multiple rigid segments are connected by 1-DOF hinges. In compliant morphing a combination

doi: 10.7712/150123.9794.444909

of rigid segments and flexible elements is used. In both cases the system is controlled by actuators.

Part of the CleanSky 2 project MANTA focusses on the development of an active morphing winglet demonstrator, following a GKN Fokker concept [3, 4]. A morphing tab is installed at the trailing edge of the winglet as illustrated in Figure 1. The morphing tab is able to rotate around the span width direction of the winglet. This concept uses a compliant morphing principle. A flexible skin and a so-called Shear Resistant Flexure (SRF) - that replaces the function of a system of hinges - characterize the morphing winglet design innovation of the AEROMO2 project. The actuator and flexible skin create the function of bending the morphing tab. The SRF prevents that aerodynamic loads (F_{aero}, Figure 1B) cause large out-of-plane deformations of the morphing tab, and therefore needs to be shear-resistant while allowing for bending of the movable. Within MANTA, an AEROMO2 project is defined, focusing on the development and the design of this SRF. This paper investigates the different steps necessary to develop the SFR for the winglet demonstrator, though it could be used for any other flexibles following the described principle. The combination of a flexible skin and an SRF are promising for noise reduction and a smoother air flow which reduces drag. Both the flexible skin as the SRF are made from composite material consisting of a woven fabric and a thermoplastic matrix. The SRF to be designed should fulfill a list of constraints that could seem contradictory. It should be bending compliant around the z-axis (Figure 1) while sustaining the large deformation necessary for the rotation of the movable, though being shear stiff in the x-y plane to counteract the aerodynamical loads and guarantying a continuous skin deformation. Additionally it should be able to withstand a number of cycles representative of the lifetime of the aircraft without showing any fatigue damage.

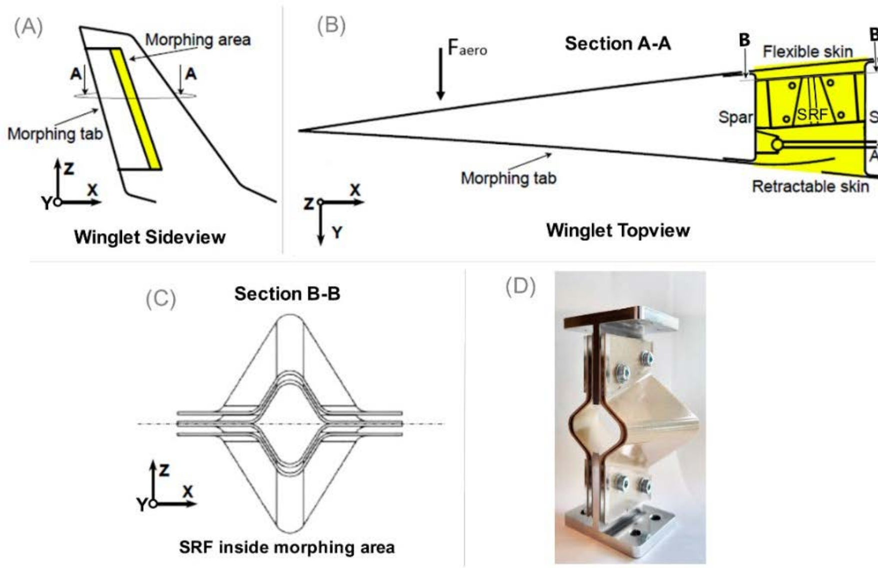

Figure 1: A schematic overview of the morphing winglet. (A) Winglet sideview; (B) Winglet Topview; (C) the Shear Resistant Flexure (SRF) inside the morphing area; (D) 3D image of the SRF in its final version

In this paper the SRF is analyzed to determine where, when and how failure occurs, followed by a parametric study to determine which shape a well-functioning SRF should have.
The design methodology used to design a SRF is summarized in the diagram shown in Figure 2. This figure is also representative for the structure of the paper. The main characteristics and requirements, the SRF should comply to, are summarized in the next section. Section 3 shows the results of a preliminary study based on a first design meant to highlight the critical areas of the shells where damage occurs. The results of this study dictates the main direction for a detailed material damage model, which is developed in section 4. The material model is then used as basis for a Finite Element Analysis based parametric study, leading to the definition of a SRF. This solution was then produced and validated, as reported in section 6.

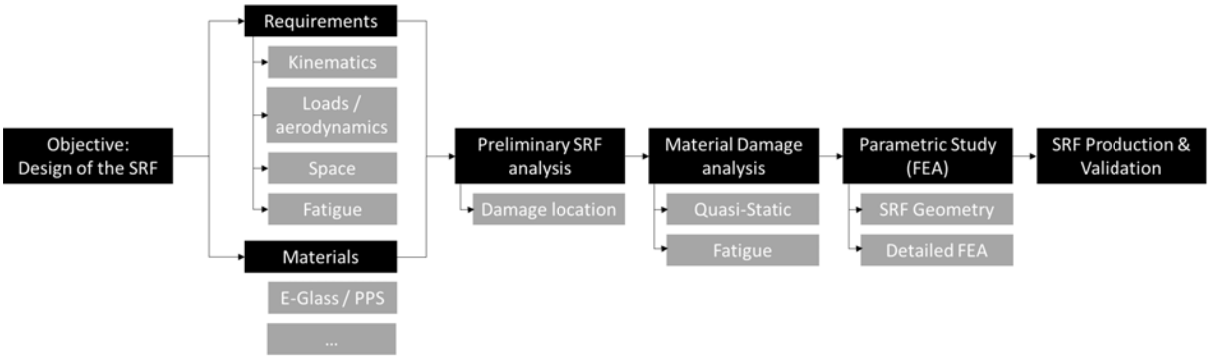

Figure 2: Schematic overview of the methodology reported in this paper

2 SHEAR RESISTANT FLEXURE

Previously performed studies within and prior to the AEROMO2 project, showed that a tapered triangular shape of the SRF is most beneficial. A triangular shape results in a high shear stiffness and a relatively low bending stiffness [5, 6]. The general shape of the SRF with parametric dimensions is shown in Figure 3. The morphing winglet has a morphing area where a series of at least two and max. four SRF shells are coupled to each other in mirrored direction and assembled to the spars of the morphing winglet (Figure 1).

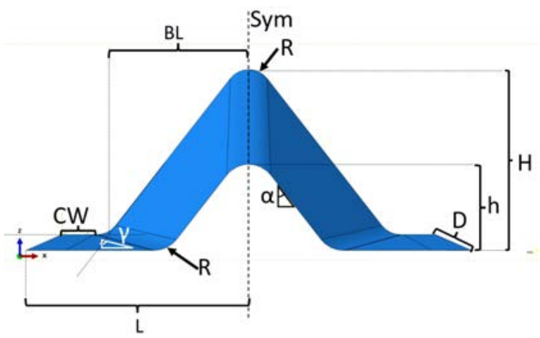

Figure 3: Picture of the general shape of the FE model of the Shear Resistant Flexure (SRF)

The to be developed SRF should comply to a list of requirements defined by the MANTA group. The resulting sets of SRFs will then be part of a full scale winglet demonstrator. The requirements cover kinematic, loading and space constraints. The SRF should allow for a bending range of the movable from -10° to +10° (kinematic requirement). It should have a shear stiffness of min. 750N/mm and a bending stiffness of max. 4200 Nmm/° and should be able to undergo the ultimate shear load of 2000N once in its lifetime without complete failure (load requirements). The outer dimensions of the SRF are max. 80 mm x 45 mm (2L x D, Figure 3) ensuring it fits between the spars and the skin without touching the skin (space requirement). The SRF should be able to withstand 120.000 full movement cycles without showing a service life degradation. This is quantified by a maximum stiffness decrease of 10% (fatigue requirement). It was chosen in an early stage to keep a material and production process qualified in the aircraft industry, i.e. a woven glass reinforced thermoplastic (PPS), able to sustain large deformations, and producible into complex shapes with a suited productivity. Laminates made of Toray TC1100 Woven 8HS E-Glass-PPS were first consolidated as flat laminates, before being thermoformed into the desired shape. The most relevant properties of this material is reproduced in Table 1.

Table 1: Overview of the material properties [7]

PROPERTY	VALUE	UNIT
Tensile Strength 0°	494	MPa
Tensile Modulus 0°	21,2	GPa
Tensile Strength 90°	369	MPa
Tensile Modulus 90°	20,0	GPa
Compression Strength 0°	470	MPa
Compression Strength 90°	316	MPa

3 PRELIMINARY STUDY

Preliminary studies within the AEROMO2 project showed that the SRFs failed in the outer layers in the corner of the shell, as depicted in Figure 4A. The loading of an SFR, bending and shear, induces folding and unfolding of the corners. When unfolding such a corner, compressive strains are induced in the outer layers of the corner. Under these conditions, further observations indicated a gradual damage development, whereby local satin woven yarns would first buckle (Figure 4B), followed by fracture of the yarn (Figure 4C). A schematic representation of this meso-damage is proposed in Figure 4E. At higher load, a series of these mechanisms leads to a gradual increase of the number of yarn fracture (Figure 4C), eventually decreasing the structural capacity of the shell. Since damage is most critical for the SRF, the design of the SRF is mainly focused on shape optimizations such that the strains in the SRF are below the (fatigue) critical strains. Based on previously performed studies within the AEROMO2 project, a $[(0,90)]_{2S}$ layup gives the most sufficient results for fatigue.

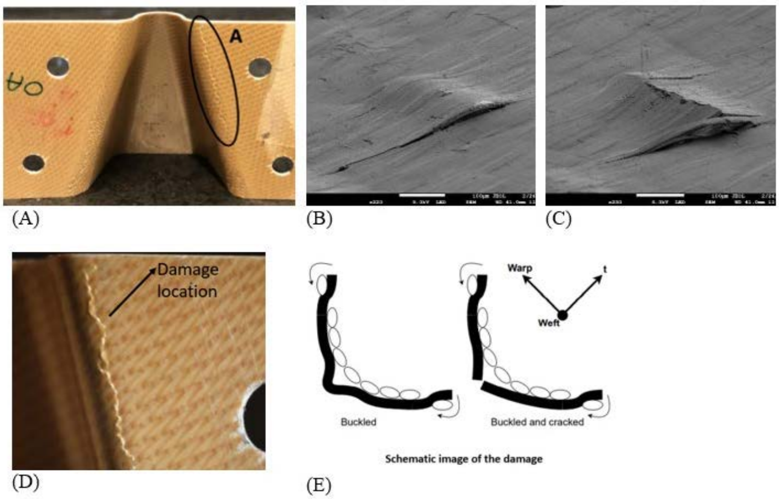

Figure 4: Compression damage at the corner (fillet) of the SRF. NB tests performed on original GKN Fokker Aerostructures SRF design.

For the design of the SRF, 120.000 full movement cycles are required within the bending range from -10° to +10°. Figure 5 shows Finite Element contour plots in fiber direction at the bottom ply of the SRF in bent position. Here blue are compression strains, red are tensile strains and green are no strains. It can be seen that the corners of the SRF have the highest strain concentrations, which is in line with the strain damage locations found in experiments. This preliminary study therefore led to the conclusion that accurate strain limits should be determined. The strain level leading to the occurrence of yarn buckling is seen as particularly important, in contrast to strains level leading to full compressive fracture as given in the material data sheet.

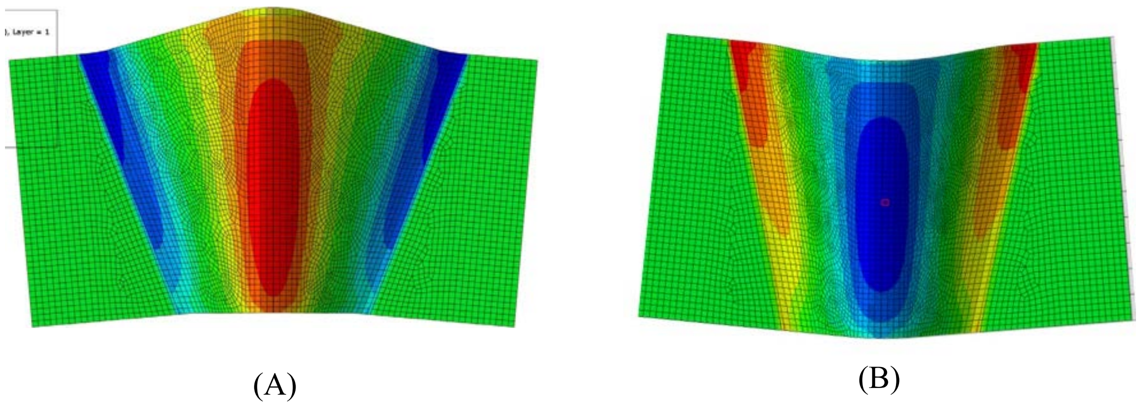

Figure 5: Contour plot of the strains at the bottom ply FE model of the SRF in +10° tensile bent position (A) and in -10° compression bent position (B).

4 DAMAGE MATERIAL MODEL DEVELOPMENT

Based on the findings summarized in previous chapter of the paper, a study was initiated for the main objective to develop a quantitative damage material model. The strain levels necessary to initiate local yarn buckling were sought after. A test geometry was designed for this purpose, able to reproduce the main loading applied to the material, though on a smaller scale with a well-defined strain field. The test concerns a 2D corner, produced under the same conditions as the SRFs, and able to be loaded under unfolding and folding loading by applying a line load in respectively tensile and compression load. The test setup and specimen are shown in Figure 6, showing from left to right the Quasi-Static, the fatigue setup and the nominal geometry of the 4-layers specimen.

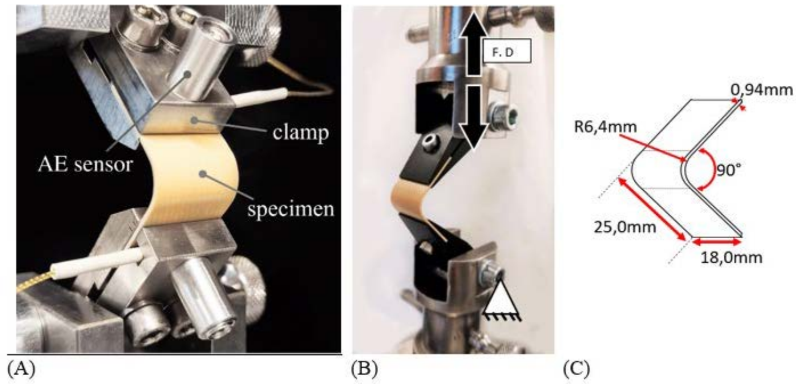

Figure 6: Corner folding and unfolding setups, Quasi-Static (A), Fatigue (B); Detail dimensions (C)

4.1 Specimen preparation

Test specimens were stamp formed 8HS Glass/PPS $[(0,90)]_{2s}$ blanks with size 100*120mm. The blanks are preheated in an IR oven at 390°C for 90s, leading to a blank mid plane temperature of 320°C. The stamp forming pressure is set at 80 bar and pressed for 60s. The tool temperature of the metal molds is 200°C. The samples are – once cooled – cut into L-shaped samples – with dimensions as shown in Figure 6C.

4.2 Test setup corner tests

Tests specimens are clamped on both sides using dedicated clamps. Each of these clamps can rotate freely in a fork, which are connected to the machine. Both test conditions used the same clamping conditions, fixed with a torque of 2Nm. The test configuration makes it possible to both fold or unfold the specimen. The quasi-static corner tests are performed on a Zwick universal testing machine with an AE-sensor integrated in each clamp (Figure 6A) while in direct contact with the material [8]. Only unfolding of the specimen was studied under these conditions. The corner fatigue tests are tested with an Instron Electropuls E1000 machine. Under fatigue conditions, 140000 cycles were performed alternating unfolding and folding. A detailed FE model (Abaqus) of the corner sample and the setup provides a relation between machine displacement and compressive strain on the surface of the outer radius. A typical result for both folding and unfolding conditions is shown in Figure 7 – in which the location where the strain is measured is marked with a red dot. The fatigue tests are performed at the compression strains: 6000με, 9000με and 12000με.

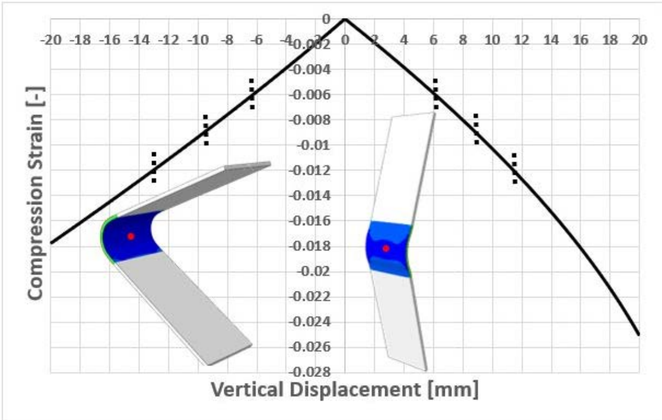

Figure 7: Strain - displacement relation of a corner specimen

4.3 Corner sample Quasi-Static test

The quasi-static tests aimed at obtaining a detailed picture of the damage development under unfolding conditions are reported in much details by Sitohang [8]. The type of test described was able to reproduce the type of damage put forward in section 3 while testing the SRF under representative conditions. Besides, the use of Acoustic Emission in combination with detailed microscopy showed that in the case of the $[(0,90)]_{2s}$ layup, the yarn buckling damage was initiated by intra-yarn cracks occurring at a compression strain of 8000με. Figure 8 shows a cross-section showing the intra-yarn crack occurring, prior to the yarn buckling mechanism.

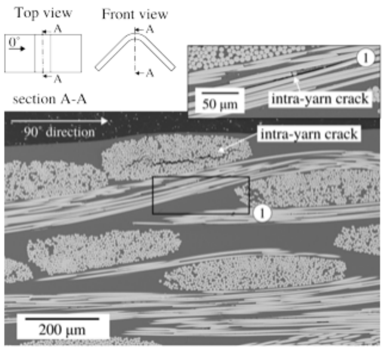

Figure 8: SEM images of [(0,90)]2s corner samples after initiation of yarn-level damage [8]

4.4 Corner sample fatigue results

Long-term cyclic tests were performed on the corner specimen at max compression strain level of 6000με, 9000με and 12000με. Samples of five specimens were tested for each condition. It is worth reminding that the strain level at which yarn damage is initiated under quasi-static conditions was measured at 8000με. The cyclic tests were monitored by analyzing regularly the force-displacement slope of the corner. It is thereby assumed that the change in slope is representative for the development of damage on the micro (fiber-matrix) and meso (yarn) level.

A summary of the fatigue test results is given in Table 2, as the average amount of cycles reached at 95 and 90% of the initial slope. The results are graphically shown in Figure 9.

Table 2: Test results of compression strain cyclic tests (average over 5 specimens and St. Dev)

STRAIN	NUMBER OF CYCLES AT 95% INITIAL SLOPE	NUMBER OF CYCLES AT 90% INITIAL SLOPE	PERCENTAGE INITIAL SLOPE AT 140.000 CYCLES
-12000με	2450 (860)	11380 (5041)	-
-9000με	25400 (14122)	>140000 (-)	92.5 (1.2)
-6000με	~135500 (~9000)	>140000 (-)	95.2 (0.2)

For the active winglet case considered, the SRF should be able to be sustain at least 120.000 cycles while staying within 90% of its initial slope. The results presented that 12000με leads to an early deterioration of the structural capacity of the material. The tests at 9000με fulfill the requirement. Still, it was chosen to keep the max strain level used for the further design to the 6000με level, in order to stay on the conservative side. A validation of this results on cyclic testing of the SRF is yet to be performed.

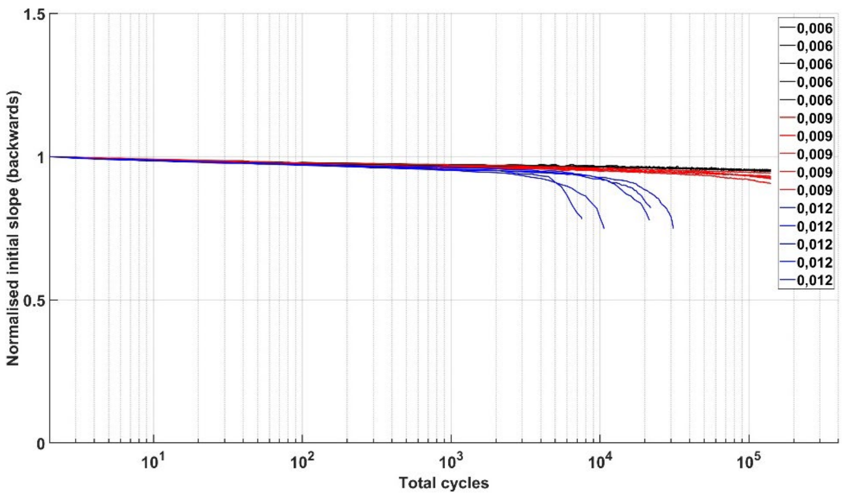

Figure 9: Normalized initial stiffness slope versus the total number of cycles for the corner specimen tests at 12000 με; 9000 με and 6000με compression strain levels

5 PARAMETRIC STUDY NEW SRF

The corner study showed that a compression strain of approximately 6000με at the outside of the corner is required to meet the 120.000 cycles requirement with less than 90% stiffness reduction. By using python scripting for Abaqus, a parametric study is performed to optimize the shape of the SRF. A simple, shell based model is used for this purpose. Four of the parameters shown in Figure 3, are varied. Table 3 shows an overview of the parameters that are studied. Since one parameter is varied at the time, the fixed values are the values used when that parameter is not varied at that moment. The dependent or unvaried parameters as used in the parametric study are shown in Table 4. The results of the parametric study are shown in Figure 10 up to and including Figure 13 for the case four SRFs are coupled on a single spot. It can be seen that the compression strain and stiffness curves are approximately parallel to each other when varying the parameters. It means that, when the surface area of the SRF increases, the compression strain decreases as well as the shear stiffness. It is chosen for optimization to use parameter values that give the highest shear stiffness without crossing the 6000με strain limit, which means making the surface area as large as possible without having a shear stiffness less than 750N/mm. The dimensions chosen are given in the last column of Table 3.

Table 3: Overview of the independent varied parameters and its range

PARAMETERS	FIXED VALUES	UNIT	LOWEST	HIGHEST	CHOSEN
Bottom length (*BL*)	30.0	mm	22	34	28.3
Alpha (.)	30.0	°	24	36	31
Gamma (γ)	19.0	°	15	25	16
Radius (*R*)	5.0	mm	4	7	5

Table 4: Overview of the dependent or unvaried parameters

PARAMETERS	FORMULA / VALUE	UNIT
H	*BL*/tan(α)	mm
h	(*BL*-*D**tan(γ))/tan(α)	mm
CW	*L*-*BL*-(*R*/tan((90+α)/2))	mm
L	40	mm
D	45	mm
Number of plies	4	-

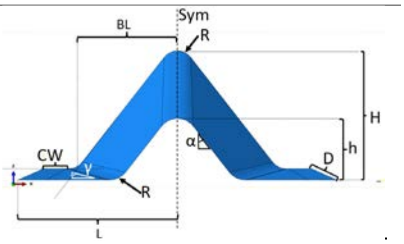

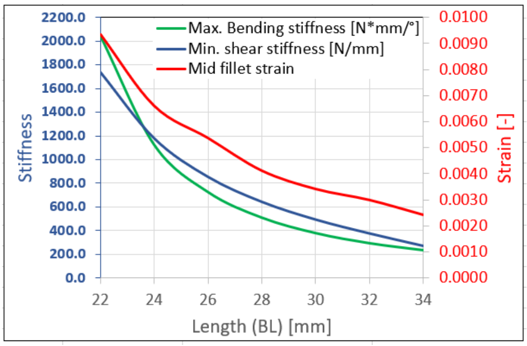

Figure 10: Stiffness and strain plot for as a function of the parameter bottom length (BL)

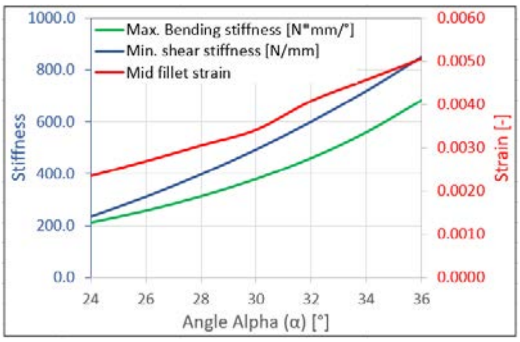

Figure 11: Stiffness and strain plot as a function of the parameter angle alpha.

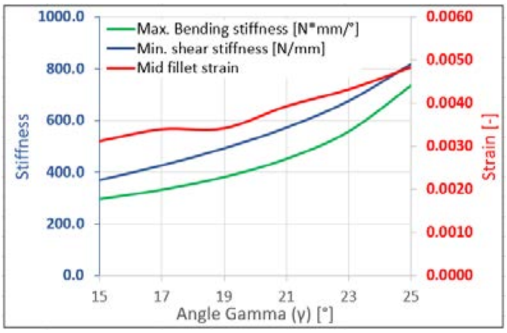

Figure 12: Stiffness and strain as a function of the parameter angle gamma

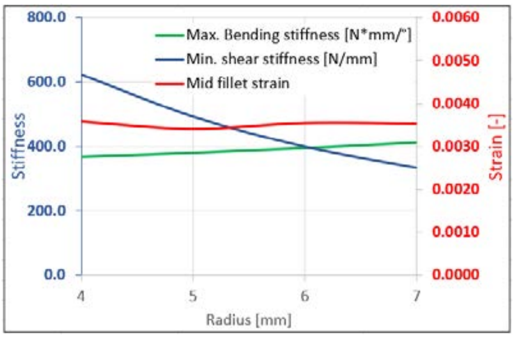

Figure 13: Stiffness and strain as a function of the parameter radius.

6 EVALUATION OF THE NEW SRF

A series of SRFs are stamp-formed using the same method as for the corner samples. A testing setup representing a section of the winglet is designed and built in order to validate the design proposed. This section summarizes the main results obtained.

6.1 SRF test setup

The testing setup, as sketched in Figure 14, is able to apply both bending as aerodynamical load induced shear load to a combination of a SRF and section of a skin (250mm width) [9]. It uses for this purpose a servo-hydraulic MTS machine meant to apply the +10° / -10° bending of the skin, in combination with a pneumatic actuator for the shear load. A dedicated deformation measurement device based on a laser line and a CCD camera is used to control the effectivity of the SRF to prevent the shear deformation.

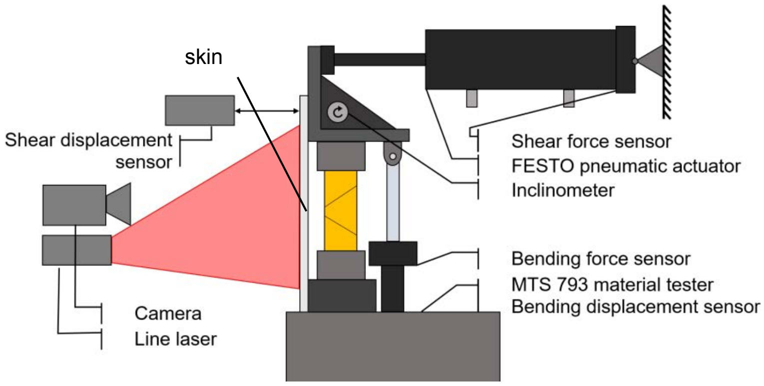

Figure 14: Test setup of the SRF [10]

6.2 SRF bending test results

The SRF is tested on a variety of loading scenarios. The combination of skin and SRF provided shear stiffness values under combined bending and shear of 1710N/mm and 2270N/mm at a angles of -10° compression bending and +10° tensile bending respectively. Both these values exceed the min. required 750N/mm, while these value stay within 20% of the simple FEM prediction used for the design. Additionally the SRF is loaded to its ultimate shear load of 2000N at -10° compression bent-and +10° tensile bent position [10]. The ultimate load test successfully reached to 2000N for the -10° compression bent state. For the +10° tensile bent state, the SRF failed in the corners at the bottom ply at a shear load of 1828N.

7 CONCLUSION

This paper shows the development of thermoplastic composite based SRFs for an application in a compliant morphing winglet. The resulting SRF concerns a shell geometry which allows large deformation while being stiff to support aerodynamical loads, thereby fulfilling kinematical, loads and space requirements.

The large deformation of the thermoplastic composites used asked for a material specific damage model. A simplified test geometry was developed for this purpose, which was able to reproduce the typical damage observed on this types of shells. It allowed the definition of strain limits, which were supported by a cyclic test program.

Finally, a FE based parameter analysis based on the measured strain limits led to the definition of a geometry for an SRF able to satisfy the requirements set for the project. The stamp formed SRFs were tested on a dedicated setup designed to apply the necessary deformation and loads. Testing showed a sufficient shear stiffness, while being able to sustain the 2000N ultimate load test at -10^o compression bending. The design failed however in the 2000N ultimate load test at +10° tensile bending. This means that some additional optimization is necessary.

ACKNOWLEDGEMENTS

The project is part of the AEROMO2 JTI-CS2-2019-CFP10-AIR-01-45 project number 887240, funded by the Clean Sky 2 Joint Undertaking.

The authors would like to thank the MSc students, M.G. de Graaf, T.J. van Rijnsoever, T. Schaap, T.N. Kneefel and J. van Donkersgoed for their contributions to this research.

REFERENCES

1 A. Concilio, I. Dimino, R. Pecora, M. Arena, ‘‘Aircraft morphing systems: elasticity of selected components and modelling issues‘‘, *Proc. of SPIE*, 11376, 2020.

2 D. Ninian, S.M. Dakka, ‘‘Design, Development and Testing of Shape Shifting Wing Model’’, *Aerospace*, vol. 4, no. 52, 2017.

3 https://www.utwente.nl/en/et/ms3/research-chairs/pt/research/aeromo2cleansky2/, accessed 05-23 2022.

4 A.M.F. Bastiaansen, ‘‘Airfoil shaped body with a variable outer shape’’, Patent NL2018538B1, 2018.

5 A. Broer, ‘‘Morphing Movable: Analysis of the Flex-Region’’, *MSc Thesis*, TU Delft, 2016.

6 M.J. Materman, ‘‘Optimization of the flexible shear element of a morphing winglet concept’’, *MSc Thesis*, University of Twente, 2021.

7 Toray Advanced Composites, ‘‘Cetex® TC1100 PPS’’, www.toraytac.com, 2021.

8 R.D.R. Sitohang, S. Benou, L.L. Warnet, R. Akkerman, ‘‘On the thickness and layup dependence of unfolding failure mechanisms in curved woven composites’’, Sent for publication to *Composites Structures*, 2023.

9 M.G. de Graaf, ‘‘Towards the application of morphing movables in a new winglet design’’, *MSc Thesis*, University of Twente, 2021.

10 J. van Donkersgoed, ‘‘Performance Characterization of a Morphing Winglet’’, *MSc Thesis*, University of Twente, 2023.